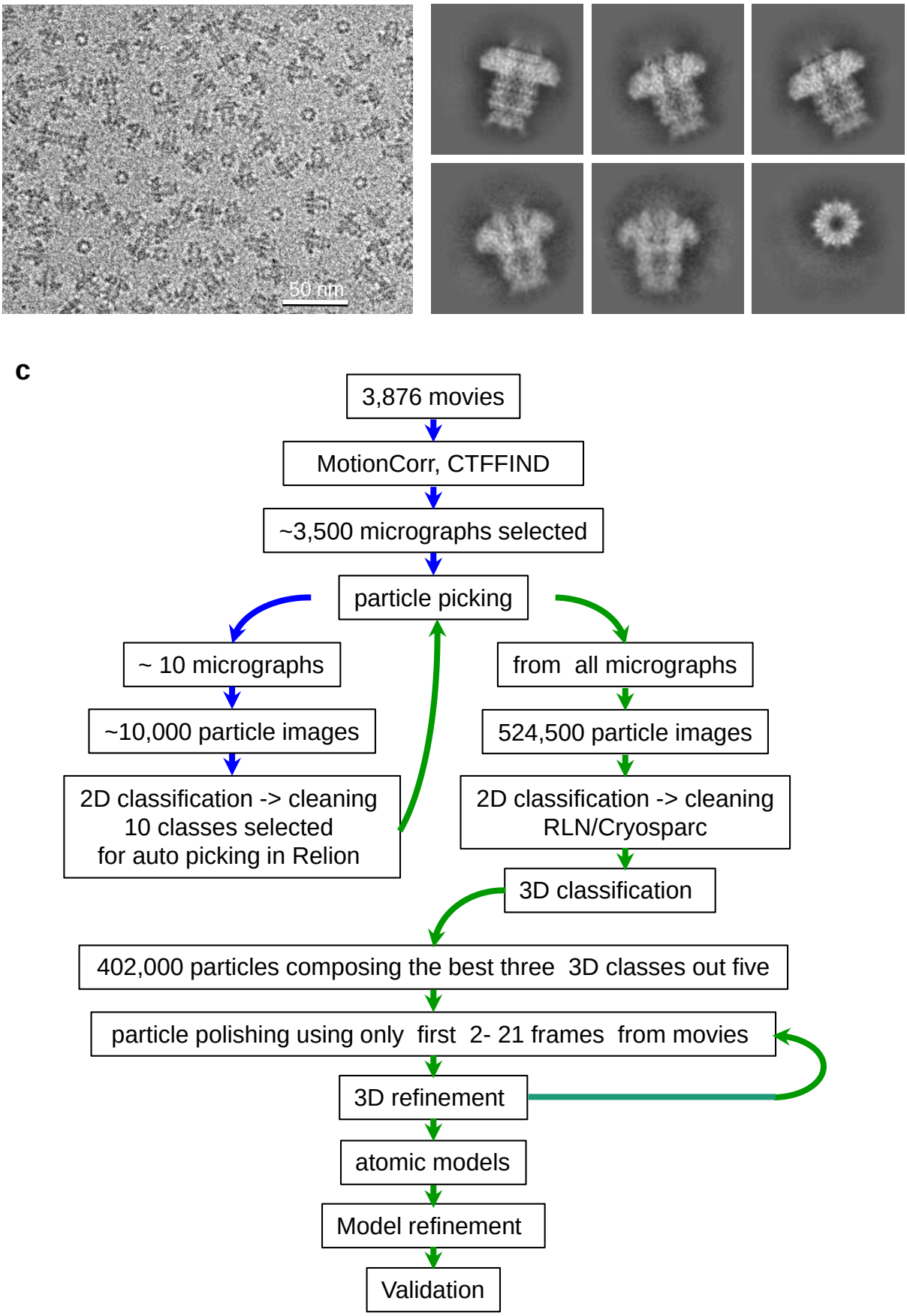

Extended Data Fig. 1 |Overall diagram of the image processing protocol.

Extended Data Fig. 1 |Overall diagram of the image processing protocol. **a**. A representative cryo-EM micrograph of the SPP1 connector. **b**. representative 2D classes of cryo-EM images of the connector (side views and one end view). **c**. The workflow of the cryo-EM image analysis, blue arrows show the link of the first steps from data collection to 2D classification and initial reconstruction. The green arrows show the work flow of the entire data set processing. The refined map of the connector complex was calculated using ~402,000 particle images.

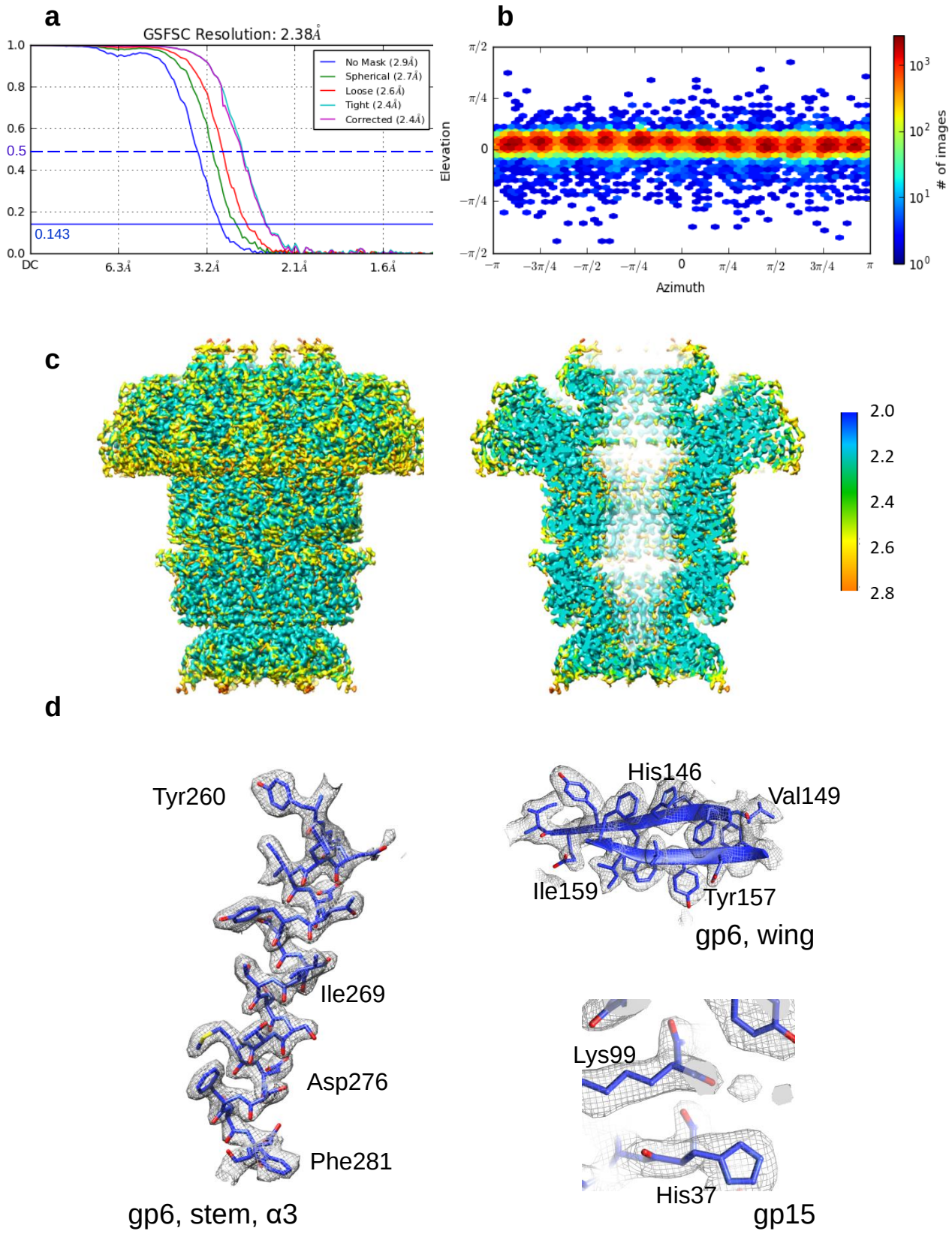

Extended Fig. 2| Assessment of the map resolution.

Extended Fig. 2| Assessment of the map resolution. a. Fourier shell correlation (FSC) curves for the SPP1 connector map. The FSC curves are calculated using different types of masks: the curve in blue is the FSC between two cryo-EM maps without any mask; the curve in green with a spherical mask; the curve in red with a loose mask; the curves in purple and cyan are FSCs between two cryo-EM maps using tight masks, and the fitted, generated, atomic model. At the threshold of 0.143 resolution was 2.38 Å, at the threshold of 0.5 it was 2.7 Å. **b.** Angular distribution of particle images used at the reconstruction. The colours indicate the number of images that have such orientations according to the bar shown on the right. **c.** The EM map of the SPP1 connector coloured according to local resolution. The middle panel displays a cut-away view of the map allowing to see the details and resolution within the connector channel. Regions at higher resolution are in cyan, regions at lower resolution are in orange. Colour bar is shown in the right panel**. d.** Examples of fitting of the atomic models into EM densities. The left panel shows fitted helix α3 of the gp6 stem domain with side chains into the EM density (grey mesh). A fitted β-hairpin of the wing domain is shown in the upper right panel. A region of gp15 with fitted residues is shown in the bottom right panel.

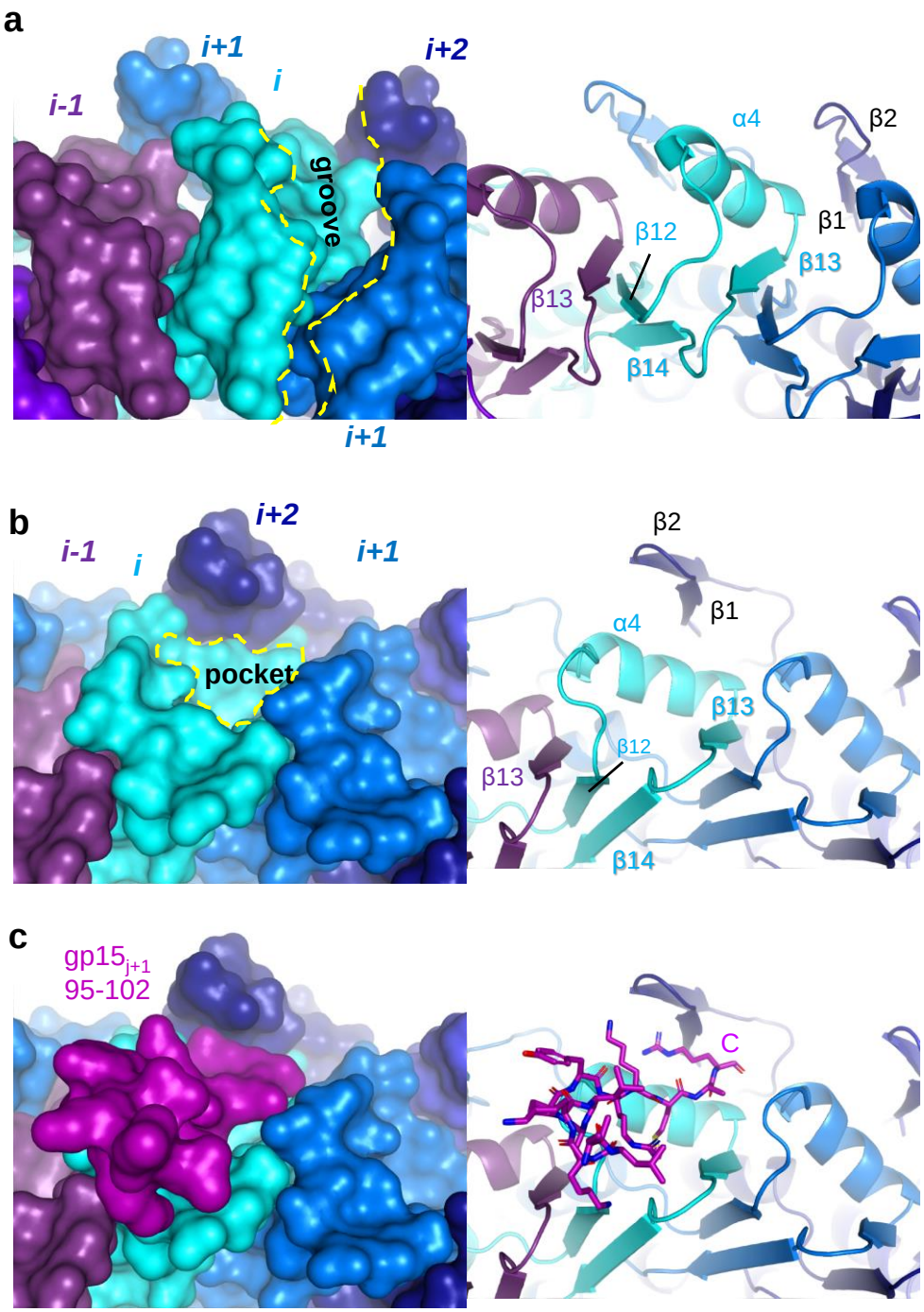

Extended Data Fig. 3 | The binding interface of gp6 and gp15 at the clip bottom.

Extended Data Fig. 3 | The binding interface of gp6 and gp15 at the clip bottom. a, Surface (left) and cartoon (right) views of three gp6 subunits in the assembly-naïve 13-mer. Secondary structure elements are labelled on the right panel and subunits are color-coded as in Fig. 1b. The 13-mer inter-subunit interface forms a groove in the clip (outlined by dashed curve in yellow). **b**, The pocket cavity is formed by three adjacent gp6 subunits *i, i+1*, and *i+2.* The area of interactions between the connector gp6 12-mer and gp15 is outlined by dashed yellow curve. **c**, Gp15 carboxyl terminus bound to the gp6 clip pocket of the connector. The last seven residues of gp15 are rendered as surface (left) and sticks (right) in magenta. All views are shown form the tail side.

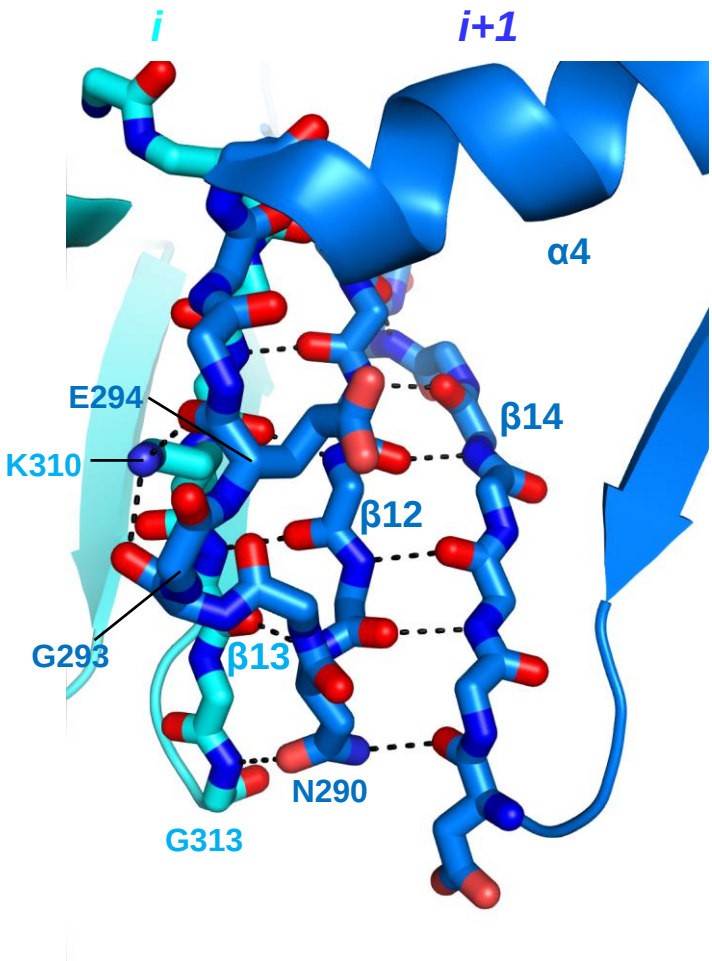

Extended Data Fig. 4 | Bonding network of gp6 clip residues N290, G293 and E294. Subunits *j* and *j+1* are coloured as in Fig. 1b. Bonds are shown by black dashed lines.

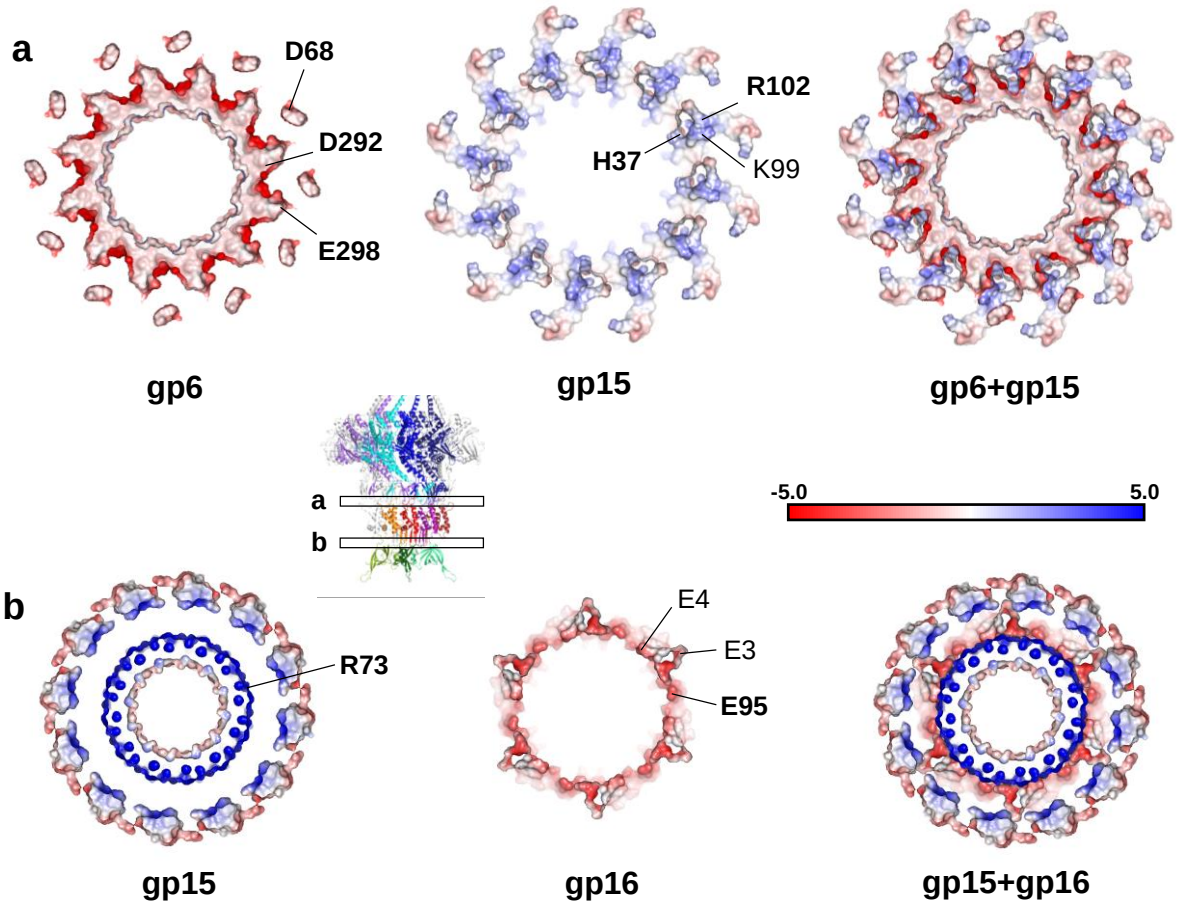

Extended Data Fig. 5 | Electrostatic potential at the gp6-gp15 and gp15-gp16 interfaces.

Extended Data Fig. 5 | Electrostatic potential at the gp6-gp15 and gp15-gp16 interfaces. a, Slab of the local electrostatic potential of the gp6 clip bottom region (left) and its interacting gp15 interface (centre). The slab through the two proteins (right) highlights electrostatic potential complementarity and shape match. Electrostatic potentials are rendered in red and blue from -5.0 kT/e (red) to 5.0 kT/e (blue); see the scale bar in the middle of the figure on the right side. Residues establishing gp6-gp15 saline bridges are labelled in bold and charged residues are also identified. **b,** Slab of the local electrostatic potential complementarity of the gp15 (left) and gp16 (centre) demonstrates interaction interfaces at the level of Arg73 in the β-barrel of gp15 (right panel). The positions of slabs in **a** and **b** are shown in the connector view in the centre of the figure. All views are shown from the tail side.

a

protein	phage	oligo state	structure	PDB	Z-score	Reference
gp15	siphophage SPP1	12	cryoEM	7Z4W		this work
gp6	siphophage HK97	13	X-rays	3JVO	9.2	2
YqbG	skin element *B subtilis*	1	NMR	1ZTS	6.4	3
gp36	myophage Mu	1	NMR	5YDN	6.4	4
gp11	podophage T7	12	cryoEM	6R21	5.3	5
gp15	siphophage SPP1	1	NMR	2KBZ	4.1	6
Distant homologues:						
gp4	podophage P22	12	X-rays	4V4K		7
lower collar	podophage P68	12	cryoEM	6IAC		8
gp11	podophage φ29	12	cryoEM	6QZF		9

b

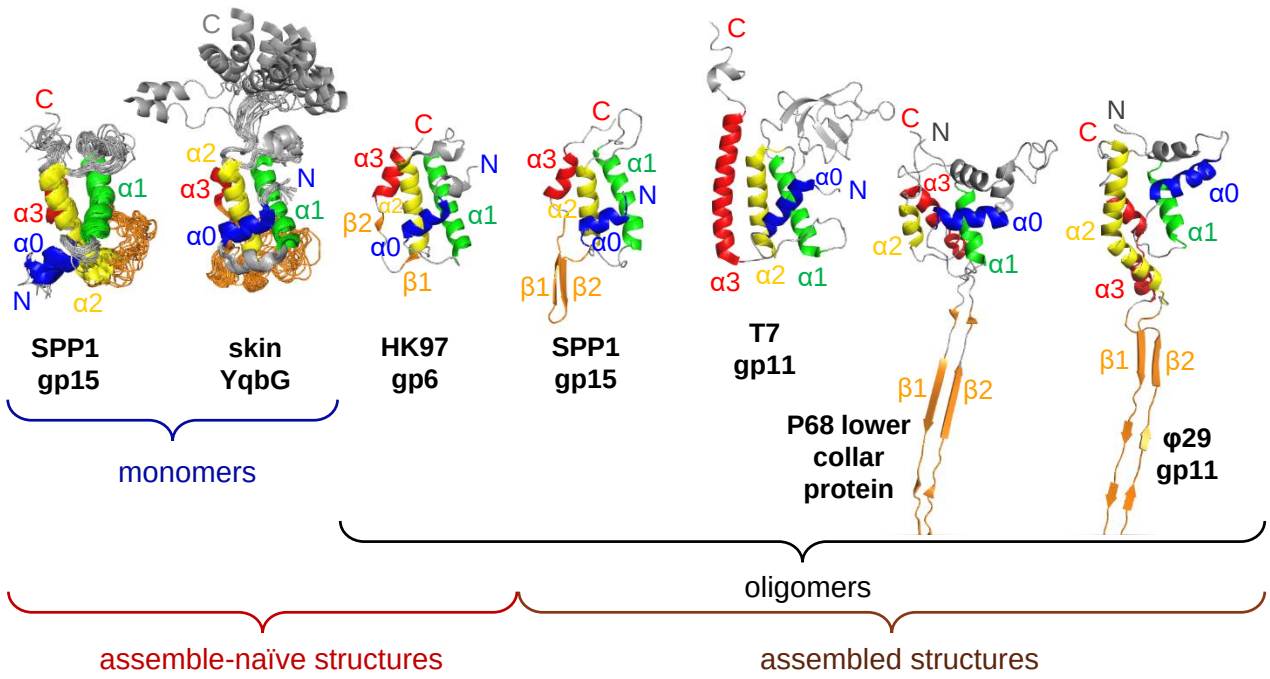

Extended Data Fig. 6 | Gp15 homologous proteins conformational landscape

Extended Data Fig. 6 | Gp15 homologous proteins conformational landscape. a, SPP1 gp15 structural homologues detected with DALI[1] (Z-scores are indicated) or identified by inspection of available structures of connector complexes in cases of more distant homologues. The state of oligomerisation, structure determination method and the PDB coordinates code are shown in the table. **b,** Atomic models of monomers (twenty superimposed NMR structures of SPP1 gp15 and of skin element YqbG), and of single subunits from oligomers of assembly-naïve (HK97 gp6) and assembled viral particles SPP1 gp15, T7 gp11, P68 lower collar protein and φ29 gp11. The structures are aligned with SPP1 gp15 of the connector through helices α1, α2 and α3. Their secondary structure elements are labeled according to the SPP1 gp15 structure and colored from blue (α0) to red (helix α3 and C-terminus). Structural elements that do not present in gp15 are shown in grey. The regions extending β1-β2 outwards from the protein core of phages P68 and φ29 are truncated.

[1]Holm, L. DALI and the persistence of protein shape. *Protein Sci.* **29**, 128–140 (2020).

[2]Cardarelli, L. *et al.* The Crystal Structure of Bacteriophage HK97 gp6: Defining a Large Family of Head–Tail Connector Proteins. *J. Mol. Biol.* **395**, 754–768 (2010).

[3]Liu, G. *et al.* NMR structure of protein yqbG from Bacillus subtilis reveals a novel α-helical protein fold. *Proteins Struct. Funct. Bioinforma.* **62**, 288–291 (2005).

[4]Iwasaki, T. *et al.* Three-dimensional structures of bacteriophage neck subunits are shared in Podoviridae , Siphoviridae and Myoviridae. *Genes to Cells* **23**, 528–536 (2018).

[5]Cuervo, A. *et al.* Structures of T7 bacteriophage portal and tail suggest a viral DNA retention and ejection mechanism. *Nat. Commun.* **10**, 3746 (2019).

[6]Lhuillier, S. *et al.* Structure of bacteriophage SPP1 head-to-tail connection reveals mechanism for viral DNA gating. *Proc. Natl. Acad. Sci. U. S. A.* **106**, 8507–8512 (2009).

[7]Olia, A. S., Prevelige, P. E., Johnson, J. E. & Cingolani, G. Three-dimensional structure of a viral genome-delivery portal vertex. *Nat. Struct. Mol. Biol.* **18**, 597–603 (2011).

[8]Hrebík, D. *et al.* Structure and genome ejection mechanism of Staphylococcus aureus phage P68. *Sci. Adv.* **5**, (2019).

[9]Xu, J., Wang, D., Gui, M. & Xiang, Y. Structural assembly of the tailed bacteriophage ϕ29. *Nat. Commun.* **10**, 2366 (2019).

a. gp6 of siphophage HK97

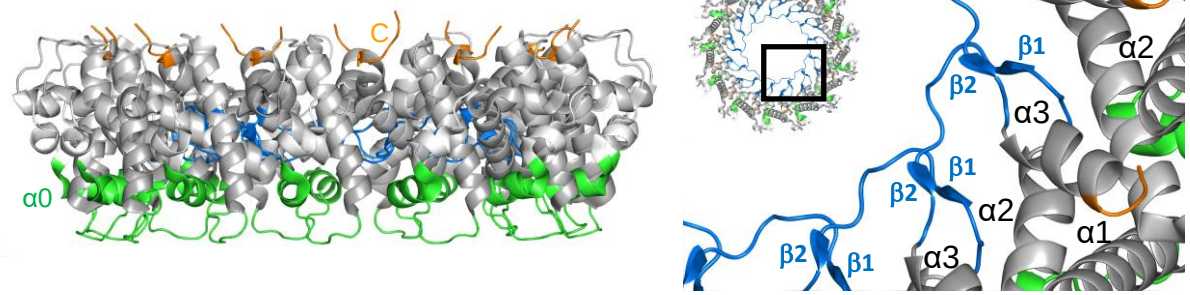

b. gp15 of siphophage SPP1

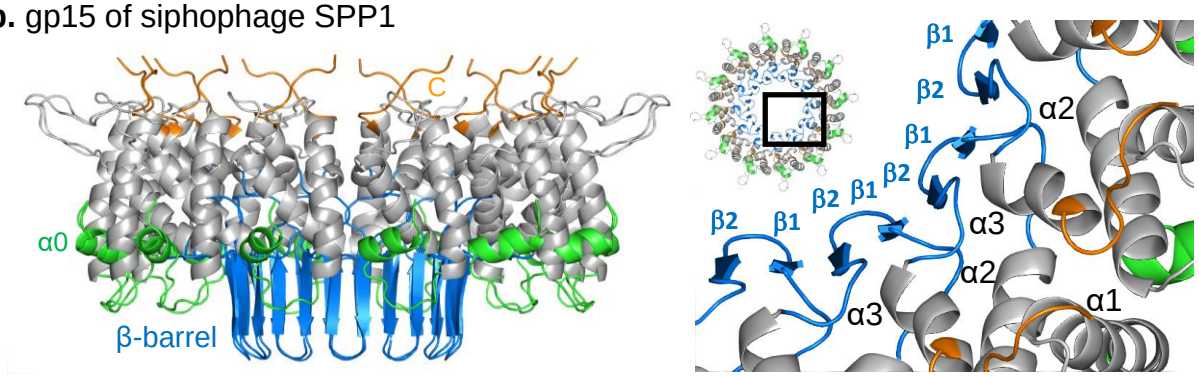

c. lower collar of podophage P68

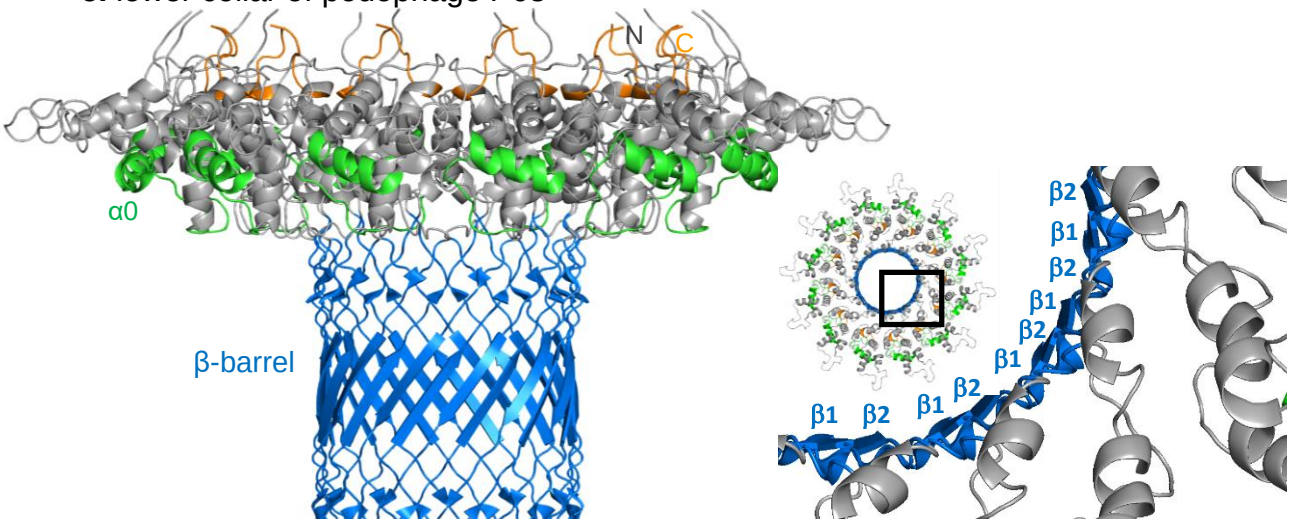

d. gp11 of podophage φ29

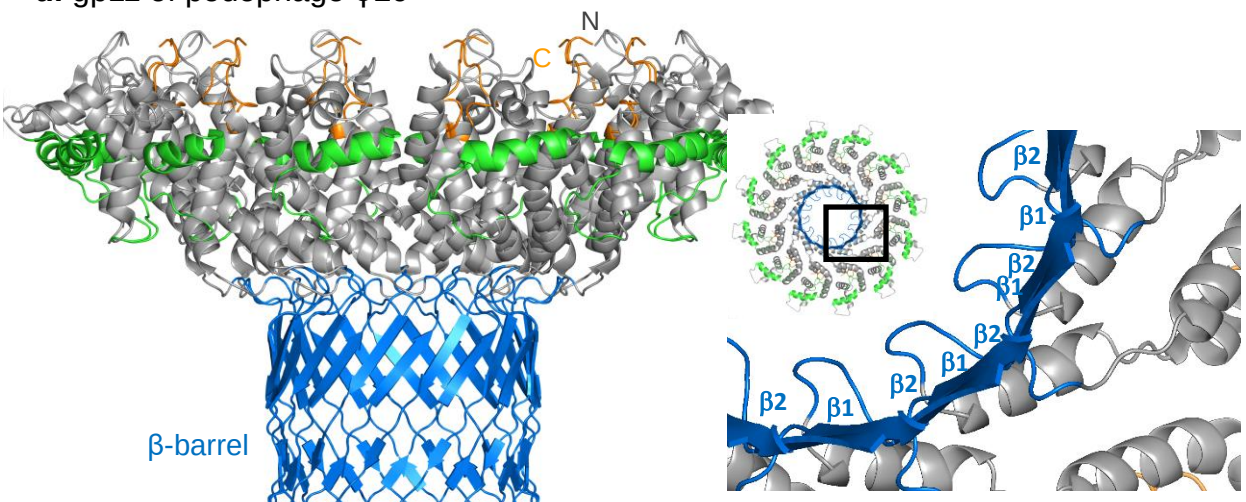

Extended Data Fig. 7 | Gp15 homologous oligomers.

Extended Data Fig. 7 | Gp15 homologous oligomers. Left panels show side views of the oligomers; right panels demonstrate end views (from the capsid) accordingly. The position of zoomed in regions are identified by rectangles in the inserts. Equivalent structural elements are shown in similar colors. The flexible C-termini that anchor these proteins to the portal complexes are shown in orange, helices corresponding to α0 are in green, and the β-barrels formed upon folding of loop α2-α3 into the β1-β2 hairpin are in blue.
a, Siphophage HK97 assembly-naïve gp6 13-mer purified from an overproducing strain[1] (PDB 3JVO), showing an anti-parallel β-like interchain interaction at the position similar to the β-barrel of structures in **b-d**. **b,** Siphophage SPP1 gp15 structure in the connector. **c,** Podophage P68 lower collar protein structure in the phage particle[2] (PDB 6IAC). The β-barrel forms the short tail DNA conduit. Its bottom part is truncated in the figure. **d,** Podophage φ29 gp11 in the phage particle[3] (PDB 6QZF). In **c** and **d** the β-barrel forms the short tail DNA conduit bottom parts of which are truncated in the figure.

[1]Cardarelli, L. *et al.* The Crystal Structure of Bacteriophage HK97 gp6: Defining a Large Family of Head–Tail Connector Proteins. *J. Mol. Biol.* **395**, 754–768 (2010).
[2]Hrebík, D. *et al.* Structure and genome ejection mechanism of Staphylococcus aureus phage P68. *Sci. Adv.* **5**, (2019).
[3]Xu, J., Wang, D., Gui, M. & Xiang, Y. Structural assembly of the tailed bacteriophage ϕ29. *Nat. Commun.* **10**, 2366 (2019).

a

protein	phage	oligo state	structure	PDB	Z-score	Reference
gp16	siphophage SPP1	6	cryoEM	7Z4W		this work
SF1141	protein from *Shigella flexneri* 2a	1	NMR	2KZ4	12.7	
XkdH	*B subtilis* phage-like element PBSX	1	Xray	3F3B	8.5	
gp16	siphophage SPP1	1	NMR	2KCA	6.1	2
gpFII	siphophage λ	1	NMR	1K0H	4.5	3
distant homologues:						
gp9	podophage φ29	6	cryoEM	6QZF		4

b

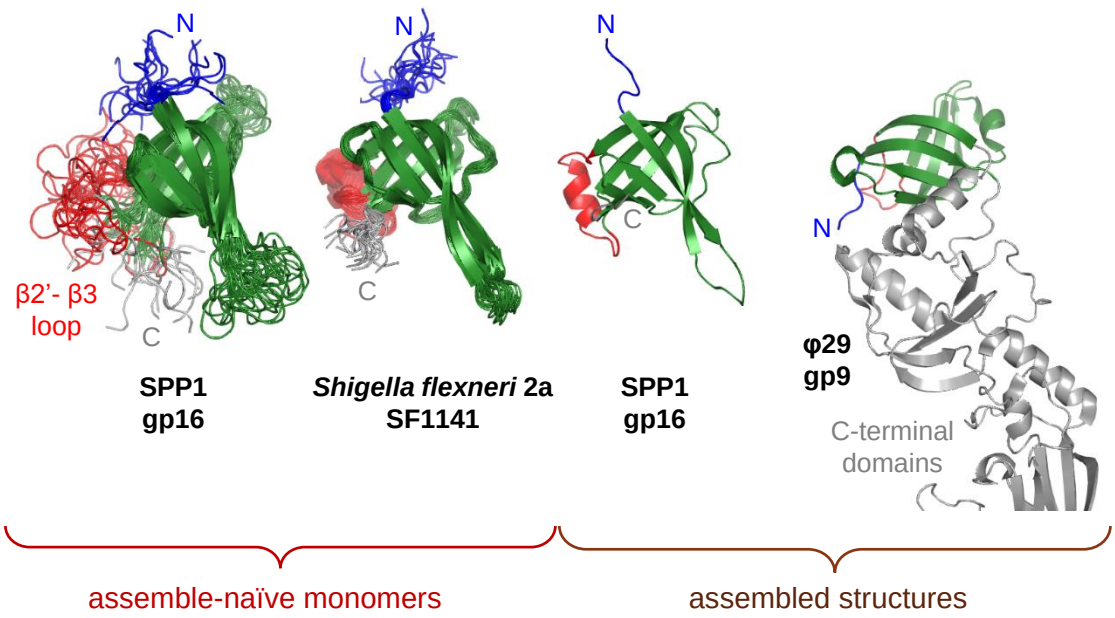

Extended Data Fig. 8 | Gp16 homologous proteins conformational landscape.

Extended Data Fig. 8 | Gp16 homologous proteins conformational landscape. a, SPP1 gp16 structural homologues detected with DALI[1] (Z-score displayed) or identified by inspection of available phage particle (sub-)structures in case of the distantly related domain of the tail knob protein gp9 from phage φ29. The oligomerisation state, structure determination method and the PDB code are indicated in the table. **b,** Atomic models of monomers (twenty superimposed NMR structures of SPP1 gp15 and of *Shigella flexneri* 2a SF1141) and of subunits from oligomers of assembled SPP1 and φ29 viral particle complexes.The structures are aligned with SPP1 gp16 through the β-barrel core. Structural elements are colored as in Fig. 4a. The N-terminal domain of φ29 gp9, which interacts with the β-barrel region of gp11 (Extended Data Fig. 7d) distal from the capsid[4], is shown in grey.

[1]Holm, L. DALI and the persistence of protein shape. *Protein Sci.* **29**, 128–140 (2020).
[2]Lhuillier, S. *et al.* Structure of bacteriophage SPP1 head-to-tail connection reveals mechanism for viral DNA gating. *Proc. Natl. Acad. Sci. U. S. A.* **106**, 8507–8512 (2009).
[3]Maxwell, K. L., Yee, A. A., Arrowsmith, C. H., Gold, M. & Davidson, A. R. The Solution Structure of the Bacteriophage λ Head–Tail Joining Protein, gpFII. *J. Mol. Biol.* **318**, 1395–1404 (2002).
[4]Xu, J., Wang, D., Gui, M. & Xiang, Y. Structural assembly of the tailed bacteriophage ϕ29. *Nat. Commun.* **10**, 2366 (2019).